frontiers | Frontiers in Chemistry

ORIGINAL RESEARCH
published: 07 April 2022
doi: 10.3389/fchem.2022.879402

First-Principles Calculations of Two-Dimensional CdO/HfS2 Van der Waals Heterostructure: Direct Z-Scheme Photocatalytic Water Splitting

Qiuhua Zhang[1], Kai Ren[2], Ruxing Zheng[2], Zhaoming Huang[3], Zongquan An[1]* and Zhen Cui[4]*

[1]School of Automobile and Aviation, Wuhu Institute of Technology, Wuhu, China, [2]School of Mechanical and Electronic Engineering, Nanjing Forestry University, Nanjing, China, [3]School of Mechanical Engineering, Wanjiang University of Technology, Ma'anshan, China, [4]School of Automation and Information Engineering, Xi'an University of Technology, Xi'an, China

Using two-dimensional (2D) heterostructure as photocatalyst for water splitting is a popular strategy for the generation of hydrogen. In this investigation, the first-principles calculations are explored to address the electronic performances of the 2D CdO/HfS_2 heterostructure formed by van der Waals (vdW) forces. The CdO/HfS_2 vdW heterostructure has a 1.19 eV indirect bandgap with type-II band alignment. Importantly, the CdO/HfS_2 vdW heterostructure possesses an intrinsic Z-scheme photocatalytic characteristic for water splitting by obtaining decent band edge positions. CdO donates 0.017 electrons to the HfS_2 layer in the heterostructure, inducing a potential drop to further separate the photogenerated electrons and holes across the interface. The CdO/HfS_2 vdW heterostructure also has excellent optical absorption capacity, showing a promising role as a photocatalyst to decompose the water.

Keywords: two-dimensional, CdO/HfS2 heterostructure, Z-scheme, photocatalyst, water splitting

OPEN ACCESS

Edited by:
Guangzhao Wang,
Yangtze Normal University, China

Reviewed by:
Wei Zhang,
Nanjing Forest Police College, China
Biao Wang,
Southwest University, China

****Correspondence:***
Zhaoming Huang
jimmymacy@163.com
Zongquan An
anzongquan@whit.edu.cn

Specialty section:
This article was submitted to Theoretical and Computational Chemistry, a section of the journal Frontiers in Chemistry

Received: *19 February 2022*
Accepted: *07 March 2022*
Published: *07 April 2022*

Citation:
Zhang Q, Ren K, Zheng R, Huang Z, An Z and Cui Z (2022) First-Principles Calculations of Two-Dimensional CdO/HfS2 Van der Waals Heterostructure: Direct Z-Scheme Photocatalytic Water Splitting. Front. Chem. 10:879402. doi: 10.3389/fchem.2022.879402

INTRODUCTION

After the discovery of graphene in 2004 as a novel two-dimensional (2D) material (Geim and Novoselov, 2007), its outstanding thermal, electronic, and mechanical properties provide remarkable applications in many fields, also promoting the development of the other 2D materials (Cui et al., 2021a; Ren et al., 2021a; Zheng et al., 2021a; Cui et al., 2021b). Acting as popular layered material, transition-metal dichalcogenides (TMDs), expressed by XM_2, where M represents transition-metal atom and X represents chalcogenide atom, is sandwiched by two chalcogenide atoms to form a sandwich structure (Hua Zhang et al., 2018). TMDs materials possess excellent electronic (Mak et al., 2010), thermal (Ren et al., 2022), thermoelectric (Wickramaratne et al., 2014), and optical (Ren et al., 2019a) performances. In recent studies, it has been proved that TMDs materials can be widely used in photocatalyst (Ren et al., 2020a), field-effect transistor (Yu et al., 2017), and photovoltaic devices (Gan et al., 2014). It is worth noting that the TMDs materials also can be prepared by an omnidirectional epitaxy (Xie et al., 2018), physical transport (Huang et al., 2014). Besides, the TMDs materials are also synthesized (Lu et al., 2017), suggesting novel photocatalytic properties (Zheng et al., 2021b; Lou et al., 2021; Zhu et al., 2021; Shao et al., 2022; Shen et al., 2022).

In recent years, using 2D materials as photocatalysts has aroused considerable focus (Wang et al., 2020a; Wang et al., 2020b; Wang et al., 2020c). The photogenerated electrons and holes in excited 2D

semiconductors can quickly move to the material surface to participate in a redox reaction, which greatly shortened the photogenerated charge moving path, and a wider reaction area is also provided (Chen et al., 2010). However, the rapid recombination between the photogenerated electrons and holes hinders the reaction efficiency (Ren et al., 2019b). To solve this obstacle, many 2D heterostructures constructed intrinsic type-II band alignment have been investigated as photocatalysts because the lifetime of the photogenerated electrons and holes can be prolonged by separating into different layers. For example, the electronic and optical properties of AlN/Bp heterostructure present type-II band arrangement and have strong light absorption ability, which has great potential in the field of photocatalytic water decomposition (Yang et al., 2017). The experimental results demonstrate that under the condition of light, g-C_3N_4/$Ca_2Nb_2TaO_{10}$ nanocomposite with a mass ratio of 80:20 has the highest hydrogen precipitation efficiency, which is more than 2.8 times that of single-layer g-C_3N_4 (Thaweesak et al., 2017). The nanorod array WO_3/$BiVO_4$ heterostructure was prepared by solvothermal technology. The experiments demonstrate that the photocatalytic performance of the heterostructure is significantly improved compared with the planar WO_3/$BiVO_4$ heterostructure. In particular, the IPCE value at 420 nm of the heterostructure film can be increased from 9.3% to 31% (Su et al., 2011). Similarly, the flower-like structure of $CoNi_2S_4$/Ni_3S_2 heterostructure was synthesized by the hydrothermal method, which shows that the electronic structure is optimized because of the high-intensity coupling between $CoNi_2S_4$ and Ni_3S_2, so as to improve the efficiency of photocatalytic water splitting (Dai et al., 2020). Furthermore, the Z-scheme photocatalyst is popular because of its extraordinary optical carrier moving path, which can provide more efficient photocatalytic performance. For example, the 2D C_7N_6/Sc_2CCl_2 heterostructure possesses ultrafast carrier recombination of about 0.74 ps, suggesting a strong redox capacity for water splitting (Meng et al., 2022). Z-scheme PtS_2/arsenene heterostructure shows a novel high solar-to-hydrogen efficiency of about 49.32% (Ren et al., 2020b). The band bending mechanism in CdO/arsenene was addressed as a potential Z-scheme photocatalyst (Ren et al., 2021b).

More recently, the layered 2D CdO was prepared by the successive ionic layer adsorption and reaction method (Shameem et al., 2017) with outstanding electronic (Zhuang and Hennig, 2013), optical (Wang et al., 2020d), and electromagnetic properties (Zhao et al., 2019), which also can be tuned by the number of layers and stacking order (Hoat et al., 2020). At the same time, the external element doping for CdO can induce magnetic moment behavior (Chaurasiya and Dixit, 2019). In addition, 2D HfS_2 was successfully prepared by the mechanical stripping method, which has attracted extensive attention from researchers (Kanazawa et al., 2016; Wang et al., 2017; Wang et al., 2019). HfS_2 has a decent carrier mobility of 1,800 $cm^2 v^{-1} s^{-1}$ (Obeid et al., 2020). Importantly, HfS_2 can be constructed into type-II heterostructure with other different 2D materials, showing an obvious quantum effect (Mattinen et al., 2019; Obeid et al., 2020). Considering the CdO and HfS_2 monolayers share the same honeycomb structure and excellent physical and chemical properties, the CdO/HfS_2 heterostructure is constructed in this report, using density functional calculations, the electronic properties of the CdO/HfS_2 heterostructure are addressed by type-II band structure. Furthermore, the direct Z-scheme photocatalytic mechanism is also investigated for water splitting. Besides, the interfacial and optical performances of the CdO/HfS_2 heterostructure are studied.

CALCULATION MODELS AND METHODS

In this study, the simulations of the first-principles calculations were performed by the Vienna *ab initio* simulation package (VASP) based on density functional theory (DFT) (Kresse and Furthmüller, 1996a; Kresse and Furthmüller, 1996b). The

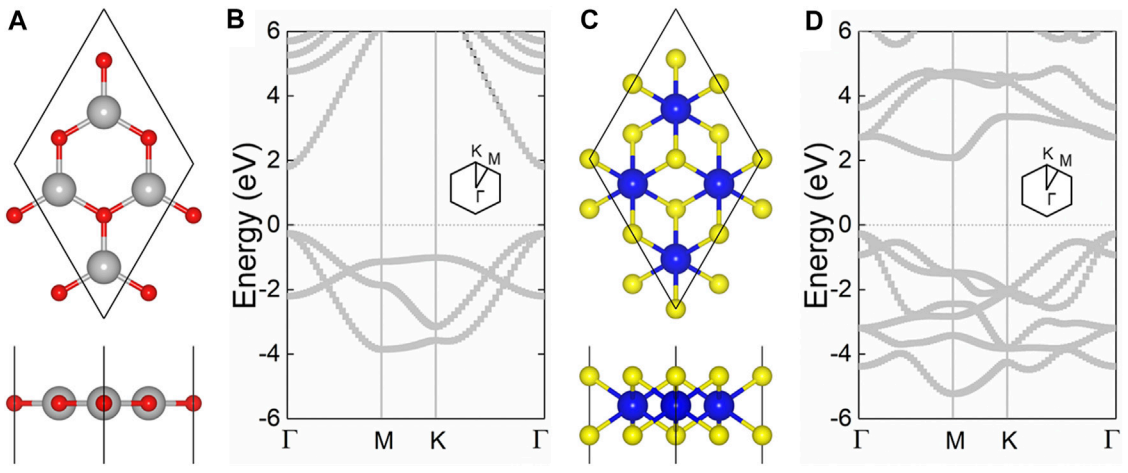

FIGURE 1 | The geometric structures of the **(A)** CdO and **(B)** HfS_2 monolayers; the band structures of the **(C)** CdO and **(D)** HfS_2 monolayers; grey, red, blue, and yellow balls are Cd, O, Hf, and S atoms, the Fermi level is set to 0.

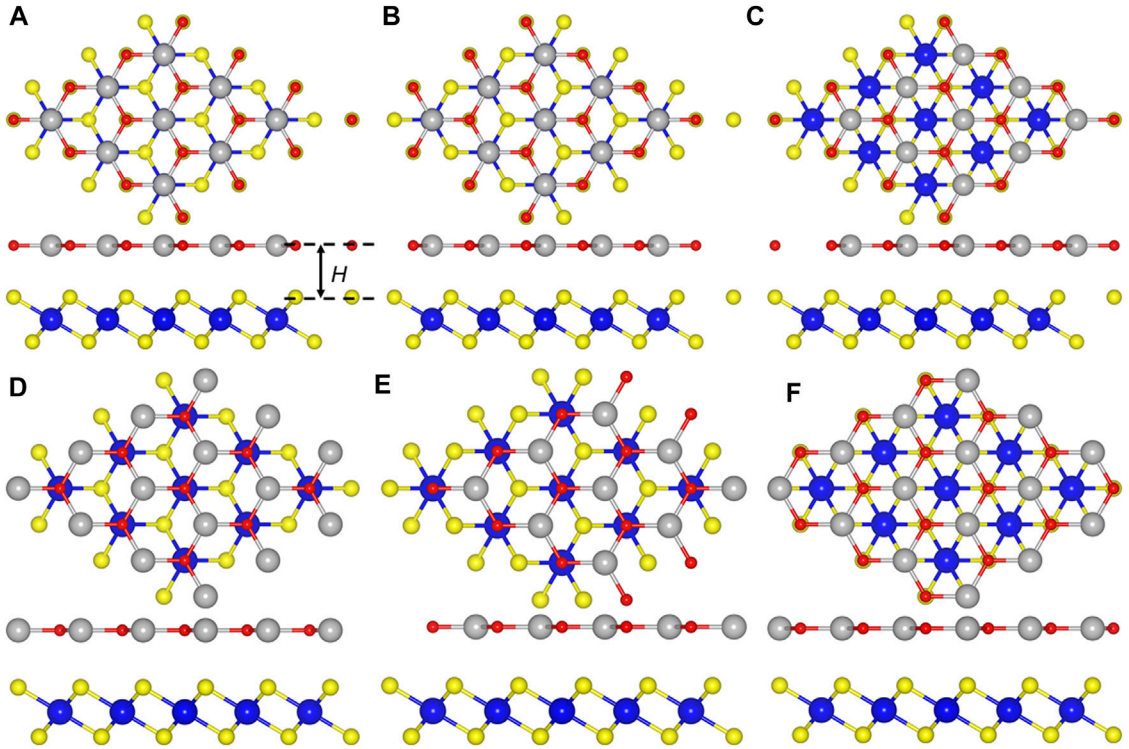

FIGURE 2 | The top and side views of CdO/HfS_2 heterostructure constructed by **(A)** CH-1, **(B)** CH-2, **(C)** CH-3, **(D)** CH-4, **(E)** CH-5, and **(F)** CH-6 configurations.

generalized gradient approximation (GGA) was considered by the projector augmented wave potentials (PAW) using Perdew–Burke–Ernzerhof (PBE) functional for exchange-correlation functional (Perdew et al., 1996; Kresse and Joubert, 1999). The DFT-D3 method was used to describe the dispersion forces using Grimme (2006). Furthermore, the Heyd–Scuseria–Ernzerhof hybrid (HSE06) calculations are explored to obtain the electronic and optical characteristics (Heyd et al., 2003). In the first Brillouin zone, the energy cut-off was used by 550 eV, and the Monkhorst–Pack *k*-point grids were set as 17 × 17 × 1. In addition, 25 Å vacuum space was considered in this investigation. The force and energy were limited within 0.01 eV $Å^{-1}$ and 0.01 meV, respectively, for convergence.

RESULTS AND DISCUSSION

The hexagonal honeycomb structure of the CdO and HfS_2 monolayers are optimized by the lattice parameters of 3.68 Å and 3.64 Å, respectively, demonstrated by **Figures 1A,C**. One can see that the CdO monolayer possesses a direct bandgap by the conduction band minimum (CBM) sharing the same point of *Γ* with the valence band maximum (VBM) in **Figure 1B**. While the HfS_2 monolayer has an indirect bandgap with the CBM between the *Γ* and M, the VBM is found near the *Γ* point, as shown in **Figure 1D**. Besides, the HSE06 obtained bandgaps of the CdO and HfS_2 monolayers are 2.07 and 2.05 eV, respectively. The results are in good agreement with the previous studies (Wang et al., 2020d; Obeid et al., 2020; Zhang and Ji, 2020).

TABLE 1 | The calculated binding energy (*E*, eV), bond length (*L*, Å), and the thickness of interface (*H*, Å) of the optimized CdO/HfS_2 heterostructure constructed by different stacking styles.

	E	L_{Hf-S}	L_{Cd-O}	*H*
CH -1	−38.08	2.58	2.18	3.23
CH -2	−42.29	2.58	2.17	2.97
CH -3	−38.71	2.58	2.18	3.18
CH -4	−41.36	2.57	2.17	3.03
CH -5	−43.93	2.57	2.17	2.86
CH -6	−41.40	2.58	2.18	3.04

The CdO/HfS_2 heterostructure is constructed in a vertical direction expressed by six different representative stacking configurations shown in **Figure 2**. We select the most stable stacking style by calculating the binding energy (*E*), which is obtained by $E = (E_h—E_{CdO}—E_{HfS2})/S$, where E_h, E_{CdO}, E_{HfS2}, and *S* represent the energy of the CdO/HfS_2 heterostructure, original CdO, HfS_2 monolayers and the area of the CdO/HfS_2 heterostructure, respectively. Importantly, the obtained lowest binding energy is about −43.93 meV/$Å^{-2}$ for CH-5 configuration, which is smaller than that in graphites of about −18 meV $Å^{-2}$, revealing van der Waals (vdW) interactions between the interface of the heterostructure (Chen et al., 2013). Moreover, the following investigations of the CdO/HfS_2 heterostructure are based on such a CH-5 configuration. Besides, the thickness of the interface of the

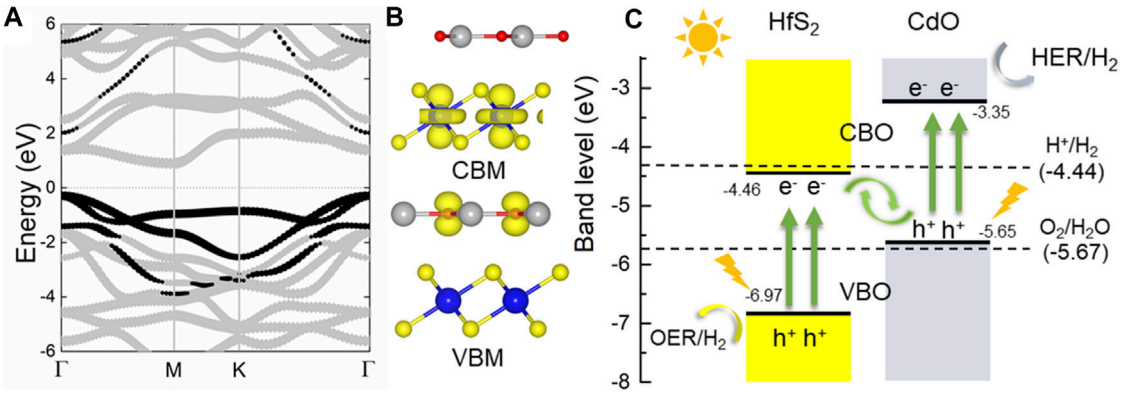

FIGURE 3 | The **(A)** projected band structure, **(B)** band-decomposed charge densities, and **(C)** band alignment of the CdO/HfS_2 vdW heterostructure compared with the oxidation and reduction of water splitting at pH 0; the Fermi level is set to 0.

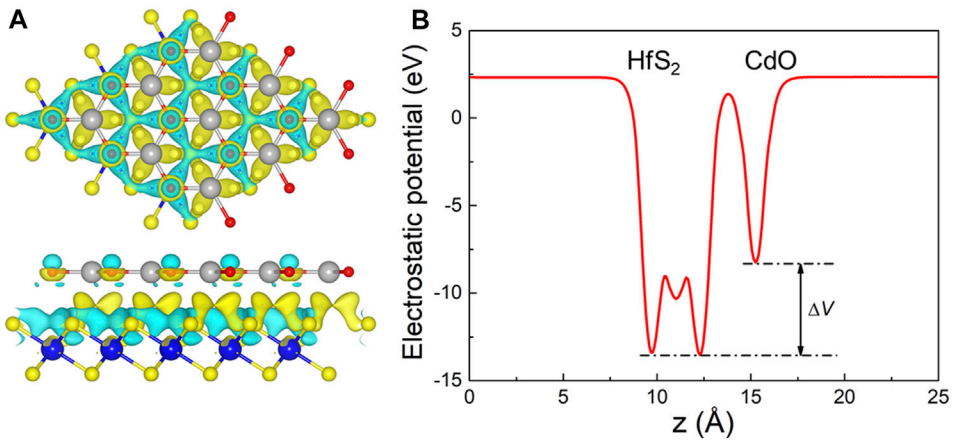

FIGURE 4 | (A) The charge density difference and **(B)** potential drop at the interface of the CdO/HfS_2 vdW heterostructure; the yellow and cyan regions mean the gaining and the loss of the electrons, respectively; the isosurface level is used as 10^{-4} |e|.

CdO/HfS_2 vdW heterostructure, explained by **Figure 2A**, is 2.86 Å, which is comparable with that of other vdW heterostructures such as ZnO/GaN (2.41 Å) (Ren et al., 2020c), BlueP/GeC, and BlueP/SiC (2.99 Å) heterostructures (Ren et al., 2019c) **Table 1**.

Next, the electronic property of the CdO/HfS_2 vdW heterostructure is explored by the projected band structure in **Figure 3A** with an indirect bandgap of 1.19 eV. The black and gray marks show the contribution of the band energy from CdO and HfS_2 monolayers, respectively. Therefore, the CBM and the VBM of the CdO/HfS_2 vdW heterostructure result from the HfS_2 and CdO layers, respectively, further proved by the band-decomposed charge densities shown in **Figure 3B**, suggesting a type-II band structure in the heterostructure. This type-II band structure of the CdO/HfS_2 vdW heterostructure can induce conduction band offset and valence band offset to further promote the migration of the photogenerated charges, revealed by **Figure 3C**. When the CdO/HfS_2 vdW heterostructure is illuminated, the photogenerated electrons will move from VBM of the CdO (or HfS_2) to the CBM, resulting in holes at VBM. Some photogenerated electrons (or holes) will be promoted from CBM (or VBM) of the CdO (or HfS_2) to the CBM of the HfS_2 (or CdO) by the conduction-band offset, CBO (or valence-band offset, VBO). Moreover, the remaining photogenerated electrons at the conduction band of the HfS_2 and the photogenerated holes at the valence band of the CdO can make recombination at the interface of the CdO/HfS_2 vdW heterostructure because of that specific band energy between the −4.44 and −5.67 eV at pH 0 (Ruiqi Zhang et al., 2018). In contrast, the band edge positions of the CBM and the VBM of the CdO and HfS_2 are −3.35 and −6.97 eV, respectively, which are decent for the redox reaction for the water splitting (Xu et al., 2018). This extraordinary flow mode of the photogenerated charge suggests a Z-scheme photocatalytic mechanism in CdO/HfS_2 vdW heterostructure, which is also reported by a $MoSe_2/HfS_2$ heterostructure (Wang et al., 2019).

When the CdO and HfS_2 layers contact, charge density difference ($\Delta\rho$) occurs between the interface of the heterostructure, which is decided by $\Delta\rho = \rho_h — \rho_{CdO} — \rho_{HfS2}$,

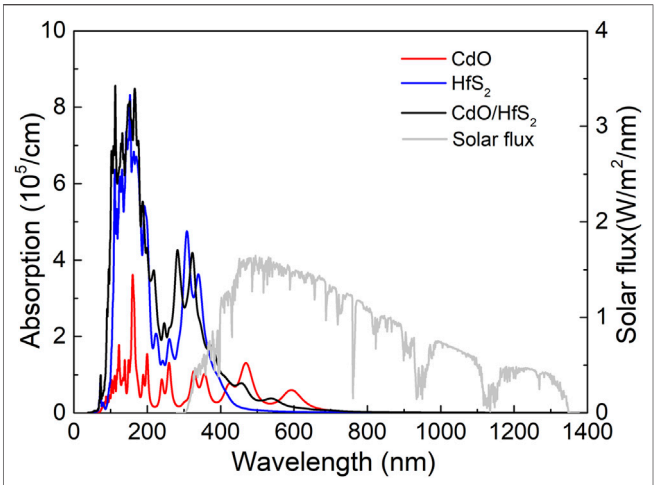

FIGURE 5 | The optical absorption spectrum of the monolayered CdO, HfS_2, and CdO/HfS_2 vdW heterostructure calculated by the HSE06 method.

where ρ_h, ρ_{CdO}, and s_{HfS2} represent the charge density of the CdO/HfS_2 heterostructure, original CdO, and HfS_2 monolayers, respectively. The charge density difference of the CdO/HfS_2 vdW heterostructure is addressed in **Figure 4A**, which shows that the electrons migrate from the CdO layer to the HfS_2 layer. The charge density amount is investigated by Bader-charge analysis (Tang et al., 2009; Sanville et al., 2007) as 0.017 electrons. Besides, the potential drop (ΔV) of the CdO/HfS_2 vdW heterostructure is also obtained in **Figure 4B** by 5.23 eV, which is larger than that of AlN/Zr_2CO_2 (0.66 eV) (Ren et al., 2021c) and Hf_2CO_2/GaN (3.75 eV) (Ren et al., 2021d). It is worth noting that this potential drop is also beneficial in promoting the separation of photogenerated charges (Wang et al., 2018).

Light absorption capacity is essential performance as a photocatalyst for water splitting. The optical absorption properties of the CdO/HfS_2 vdW heterostructure are calculated by $\alpha(\omega) = \frac{\sqrt{2}\omega}{c}\{[\varepsilon_1^2(\omega) + \varepsilon_2^2(\omega)]^{1/2} - \varepsilon_1(\omega)\}^{1/2}$, where α is the absorption coefficient. The angular frequency and the speed of light are expressed by ω and c, respectively. The real and imaginary parts of the dielectric constant are represented by $\varepsilon_1(\omega)$ and $\varepsilon_2(\omega)$, respectively. In **Figure 5**, the HSE06 obtained optical absorption spectra of the monolayered CdO, HfS_2, and CdO/HfS_2 vdW heterostructure are demonstrated by the absorption peaks of $3.56 \times 10^5\ cm^{-1}$, $4.19 \times 10^5\ cm^{-1}$, and $3.51 \times 10^5\ cm^{-1}$ at the wavelength of 342, 323, and 351 nm, respectively, in the ultraviolet region. Importantly, the CdO/HfS_2 vdW heterostructure possesses excellent visible light absorption capacity by the absorption peak of $7.21 \times 10^4\ cm^{-1}$ locating at the wavelength of 465 nm, which is higher than other reported 2D heterostructures as photocatalyst, such as g-GaN/$Mg(OH)_2$ ($5.33 \times 10^4\ cm^{-1}$) (Ren et al., 2019d) and ZnO/GaN ($4.92 \times 10^4\ cm^{-1}$) (Ren et al., 2020c). Besides, the CdO monolayer also shows a novel absorption peak of $6.01 \times 10^4\ cm^{-1}$ in the visible light spectrum of 591 nm.

CONCLUSION

In this work, the CdO/HfS_2 is constructed by vdW interactions proved by first-principles calculations. The electronic properties of the CdO and HfS_2 monolayers are calculated. In contrast, the CdO/HfS_2 vdW heterostructure possesses a type-II band structure to prevent the recombination of the photogenerated charges. Furthermore, the decent band alignment of the CdO/HfS_2 vdW heterostructure demonstrates a Z-scheme photocatalytic mechanism near the interface. Besides, the CdO/HfS_2 vdW heterostructure shows pronounced visible light absorption performance. These results explain that the CdO/HfS_2 vdW heterostructure can be used as a candidate for an excellent photocatalyst for water splitting.

DATA AVAILABILITY STATEMENT

The raw data supporting the conclusion of this article will be made available by the authors without undue reservation.

AUTHOR CONTRIBUTIONS

Conceptualization, QZ; methodology, KR; software, ZC; validation, ZH; formal analysis, ZA; investigation, KR; resources, KR, original draft preparation, QZ.

FUNDING

This work thanks the excellent top talent cultivation project in colleges and universities in Anhui province (Grant no. gxgnfx2018097), the key projects of natural science research in colleges and universities in Anhui province (Grant no. KJ 2020A0837, KJ 2020A0909), and the sub-project of national double height university scientific research platform construction and upgrading cultivation project (Grant no. Kjcxpt202005).

REFERENCES

Chaurasiya, R., and Dixit, A. (2019). Point Defects Induced Magnetism in CdO Monolayer: A Theoretical Study. *J. Magnetism Magn. Mater.* 469, 279–288. doi:10.1016/j.jmmm.2018.08.076

Chen, X., Shen, S., Guo, L., and Mao, S. S. (2010). Semiconductor-based Photocatalytic Hydrogen Generation. *Chem. Rev.* 110, 6503–6570. doi:10.1021/cr1001645

Chen, X., Tian, F., Persson, C., Duan, W., and Chen, N.-x. (2013). Interlayer Interactions in Graphites. *Sci. Rep.* 3, 3046. doi:10.1038/srep03046

Cui, Z., Luo, Y., Yu, J., and Xu, Y. (2021). Tuning the Electronic Properties of MoSi2N4 by Molecular Doping: A First Principles Investigation. *Physica E: Low-dimensional Syst. Nanostructures* 134, 114873. doi:10.1016/j.physe.2021.114873

Cui, Z., Wang, M., Lyu, N., Zhang, S., Ding, Y., and Bai, K. (2021). Electronic, Magnetism and Optical Properties of Transition Metals Adsorbed Puckered Arsenene. *Superlattices and Microstructures* 152, 106852. doi:10.1016/j.spmi.2021.106852

Dai, W., Ren, K., Zhu, Y.-a., Pan, Y., Yu, J., and Lu, T. (2020). Flower-like CoNi2S4/Ni3S2 Nanosheet Clusters on Nickel Foam as Bifunctional Electrocatalyst for Overall Water Splitting. *J. Alloys Compd.* 844, 156252. doi:10.1016/j.jallcom.2020.156252

Gan, L.-Y., Zhang, Q., Cheng, Y., and Schwingenschlögl, U. (2014). Photovoltaic Heterojunctions of Fullerenes with MoS2 and WS2 Monolayers. *J. Phys. Chem. Lett.* 5, 1445–1449. doi:10.1021/jz500344s

Geim, A. K., and Novoselov, K. S. (2007). The Rise of Graphene. *Nat. Mater* 6, 183–191. doi:10.1038/nmat1849

Grimme, S. (2006). Semiempirical GGA-type Density Functional Constructed with a Long-Range Dispersion Correction. *J. Comput. Chem.* 27, 1787–1799. doi:10.1002/jcc.20495

Heyd, J., Scuseria, G. E., and Ernzerhof, M. (2003). Hybrid Functionals Based on a Screened Coulomb Potential. *J. Chem. Phys.* 118, 8207–8215. doi:10.1063/1.1564060

Hoat, D. M., Naseri, M., Vu, T. V., Rivas-Silva, J. F., Hieu, N. N., and Cocoletzi, G. H. (2020). Structural, Electronic and Optical Properties of CdO Monolayer and Bilayers: Stacking Effect Investigations. *Superlattice. Microst.* 145, 106644. doi:10.1016/j.spmi.2020.106644

Huang, C., Wu, S., Sanchez, A. M., Peters, J. J. P., Beanland, R., Ross, J. S., et al. (2014). Lateral Heterojunctions within Monolayer MoSe2-WSe2 Semiconductors. *Nat. Mater* 13, 1096–1101. doi:10.1038/nmat4064

Hua Zhang, H., Chhowalla, M., and Liu, Z. (2018). 2D Nanomaterials: Graphene and Transition Metal Dichalcogenides. *Chem. Soc. Rev.* 47, 3015–3017. doi:10.1039/c8cs90048e

Kanazawa, T., Amemiya, T., Ishikawa, A., Upadhyaya, V., Tsuruta, K., Tanaka, T., et al. (2016). Few-layer HfS2 Transistors. *Sci. Rep.* 6, 22277. doi:10.1038/srep22277

Kresse, G., and Furthmüller, J. (1996a). Efficiency of Ab-Initio Total Energy Calculations for Metals and Semiconductors Using a Plane-Wave Basis Set. *Comput. Mater. Sci.* 6, 15–50. doi:10.1016/0927-0256(96)00008-0

Kresse, G., and Furthmüller, J. (1996b). Efficient Iterative Schemes Forab Initiototal-Energy Calculations Using a Plane-Wave Basis Set. *Phys. Rev. B* 54, 11169–11186. doi:10.1103/physrevb.54.11169

Kresse, G., and Joubert, D. (1999). From Ultrasoft Pseudopotentials to the Projector Augmented-Wave Method. *Phys. Rev. B* 59, 1758–1775. doi:10.1103/physrevb.59.1758

Lou, J., Ren, K., Huang, Z., Huo, W., Zhu, Z., and Yu, J. (2021). Electronic and Optical Properties of Two-Dimensional Heterostructures Based on Janus XSSe (X = Mo, W) and $Mg(OH)_2$: a First Principles Investigation. *RSC. Adv.* 11, 29576–29584. doi:10.1039/d1ra05521f

Lu, A.-Y., Zhu, H., Xiao, J., Chuu, C.-P., Han, Y., Chiu, M.-H., et al. (2017). Janus Monolayers of Transition Metal Dichalcogenides. *Nat. Nanotech* 12, 744–749. doi:10.1038/nnano.2017.100

Mak, K. F., Lee, C., Hone, J., Shan, J., and Heinz, T. F. (2010). Atomically ThinMoS2: A New Direct-Gap Semiconductor. *Phys. Rev. Lett.* 105, 136805. doi:10.1103/physrevlett.105.136805

Mattinen, M., Popov, G., Vehkamäki, M., King, P. J., Mizohata, K., Jalkanen, P., et al. (2019). Atomic Layer Deposition of Emerging 2D Semiconductors, HfS2 and ZrS2, for Optoelectronics. *Chem. Mater.* 31, 5713–5724. doi:10.1021/acs.chemmater.9b01688

Meng, J., Wang, J., Wang, J., Li, Q., and Yang, J. (2022). C7N6/Sc2CCl2 Weak van der Waals Heterostructure: A Promising Visible-Light-Driven Z-Scheme Water Splitting Photocatalyst with Interface Ultrafast Carrier Recombination. *J. Phys. Chem. Lett.* 13, 1473–1479. doi:10.1021/acs.jpclett.1c04194

Obeid, M. M., Bafekry, A., Ur Rehman, S., and Nguyen, C. V. (2020). A type-II GaSe/HfS2 van der Waals heterostructure as promising photocatalyst with high carrier mobility. *Appl. Surf. Sci.* 534, 147607. doi:10.1016/j.apsusc.2020.147607

Perdew, J. P., Burke, K., and Ernzerhof, M. (1996). Generalized Gradient Approximation Made Simple. *Phys. Rev. Lett.* 77, 3865–3868. doi:10.1103/physrevlett.77.3865

Ren, K., Sun, M., Luo, Y., Wang, S., Yu, J., and Tang, W. (2019). First-principle Study of Electronic and Optical Properties of Two-Dimensional Materials-Based Heterostructures Based on Transition Metal Dichalcogenides and boron Phosphide. *Appl. Surf. Sci.* 476, 70–75. doi:10.1016/j.apsusc.2019.01.005

Ren, K., Luo, Y., Wang, S., Chou, J.-P., Yu, J., Tang, W., et al. (2019). A van der Waals Heterostructure Based on Graphene-like Gallium Nitride and Boron Selenide: A High-Efficiency Photocatalyst for Water Splitting. *ACS Omega* 4, 21689–21697. doi:10.1021/acsomega.9b02143

Ren, K., Ren, C., Luo, Y., Xu, Y., Yu, J., Tang, W., et al. (2019). Using van der Waals heterostructures based on two-dimensional blue phosphorus and XC (X = Ge, Si) for water-splitting photocatalysis: a first-principles study. *Phys. Chem. Chem. Phys.* 21, 9949–9956. doi:10.1039/c8cp07680d

Ren, K., Yu, J., and Tang, W. (2019). A two-dimensional vertical van der Waals heterostructure based on g-GaN and Mg(OH)2 used as a promising photocatalyst for water splitting: A first-principles calculation. *J. Appl. Phys.* 126, 065701. doi:10.1063/1.5099125

Ren, K., Wang, S., Luo, Y., Chou, J.-P., Yu, J., Tang, W., et al. (2020). High-efficiency photocatalyst for water splitting: a Janus MoSSe/XN (X = Ga, Al) van der Waals heterostructure. *J. Phys. D: Appl. Phys.* 53, 185504. doi:10.1088/1361-6463/ab71ad

Ren, K., Tang, W., Sun, M., Cai, Y., Cheng, Y., and Zhang, G. (2020). A direct Z-scheme PtS2/arsenene van der Waals heterostructure with high photocatalytic water splitting efficiency. *Nanoscale* 12, 17281–17289. doi:10.1039/d0nr02286a

Ren, K., Luo, Y., Yu, J., and Tang, W. (2020). Theoretical prediction of two-dimensional ZnO/GaN van der Waals heterostructure as a photocatalyst for water splitting. *Chem. Phys.* 528, 110539. doi:10.1016/j.chemphys.2019.110539

Ren, K., Shu, H., Huo, W., Cui, Z., Yu, J., and Xu, Y. (2021). Mechanical, Electronic and Optical Properties of a Novel B2P6 Monolayer: Ultrahigh Carrier Mobility and strong Optical Absorption. *Phys. Chem. Chem. Phys.* 23, 24915–24921. doi:10.1039/d1cp03838a

Ren, K., Zheng, R., Yu, J., Sun, Q., and Li, J. (2021). Band Bending Mechanism in CdO/Arsenene Heterostructure: A Potential Direct Z-Scheme Photocatalyst. *Front. Chem.* 9, 788813. doi:10.3389/fchem.2021.788813

Ren, K., Zheng, R., Lou, J., Yu, J., Sun, Q., and Li, J. (2021). Ab Initio Calculations for the Electronic, Interfacial and Optical Properties of Two-Dimensional AlN/Zr2CO2 Heterostructure. *Front. Chem.* 9, 796695. doi:10.3389/fchem.2021.796695

Ren, K., Zheng, R., Xu, P., Cheng, D., Huo, W., Yu, J., et al. (2021). Electronic and Optical Properties of Atomic-Scale Heterostructure Based on MXene and MN (M = Al, Ga): A DFT Investigation. *Nanomaterials* 11, 2236. doi:10.3390/nano11092236

Ren, K., Qin, H., Liu, H., Chen, Y., Liu, X., and Zhang, G. (2022). Manipulating Interfacial Thermal Conduction of 2D Janus Heterostructure via a Thermo-Mechanical Coupling. *Adv. Funct. Mater.*, 2110846. doi:10.1002/adfm.202110846

Ruiqi Zhang, R., Zhang, L., Zheng, Q., Gao, P., Zhao, J., and Yang, J. (2018). Direct Z-Scheme Water Splitting Photocatalyst Based on Two-Dimensional Van Der Waals Heterostructures. *J. Phys. Chem. Lett.* 9, 5419–5424. doi:10.1021/acs.jpclett.8b02369

Sanville, E., Kenny, S. D., Smith, R., and Henkelman, G. (2007). Improved Grid-Based Algorithm for Bader Charge Allocation. *J. Comput. Chem.* 28, 899–908. doi:10.1002/jcc.20575

Shameem, A., Devendran, P., Siva, V., Raja, M., Bahadur, S. A., and Manikandan, A. (2017). Preparation and Characterization Studies of Nanostructured CdO Thin Films by SILAR Method for Photocatalytic Applications. *J. Inorg. Organomet. Polym.* 27, 692–699. doi:10.1007/s10904-017-0512-1

Shao, C., Ren, K., Huang, Z., Yang, J., and Cui, Z. (2022). Two-Dimensional PtS2/MoTe2 van der Waals Heterostructure: An Efficient Potential Photocatalyst for Water Splitting. *Front. Chem.* 10, 847319. doi:10.3389/fchem.2022.847319

Shen, Z., Ren, K., Zheng, R., Huang, Z., Cui, Z., Zheng, Z., et al. (2022). The Thermal and Electronic Properties of the Lateral Janus MoSSe/WSSe Heterostructure. *Front. Mater.* 9, 838648. doi:10.3389/fmats.2022.838648

Su, J., Guo, L., Bao, N., and Grimes, C. A. (2011). Nanostructured WO3/BiVO4Heterojunction Films for Efficient Photoelectrochemical Water Splitting. *Nano Lett.* 11, 1928–1933. doi:10.1021/nl2000743

Tang, W., Sanville, E., and Henkelman, G. (2009). A Grid-Based Bader Analysis Algorithm without Lattice Bias. *J. Phys. Condens. Matter* 21, 084204. doi:10.1088/0953-8984/21/8/084204

Thaweesak, S., Lyu, M., Peerakiatkhajohn, P., Butburee, T., Luo, B., Chen, H., et al. (2017). Two-dimensional G-C3N4/Ca2Nb2TaO10 Nanosheet Composites for Efficient Visible Light Photocatalytic Hydrogen Evolution. *Appl. Catal. B: Environ.* 202, 184–190. doi:10.1016/j.apcatb.2016.09.022

Wang, D., Zhang, X., Liu, H., Meng, J., Xia, J., Yin, Z., et al. (2017). Epitaxial Growth of HfS 2 on Sapphire by Chemical Vapor Deposition and Application for Photodetectors. *2d Mater.* 4, 031012. doi:10.1088/2053-1583/aa7ea2

Wang, S., Tian, H., Ren, C., Yu, J., and Sun, M. (2018). Electronic and Optical Properties of Heterostructures Based on Transition Metal Dichalcogenides and Graphene-like Zinc Oxide. *Sci. Rep.* 8, 12009. doi:10.1038/s41598-018-30614-3

Wang, B., Wang, X., Wang, P., Yang, T., Yuan, H., Wang, G., et al. (2019). Bilayer MoSe2/HfS2 Nanocomposite as a Potential Visible-Light-Driven Z-Scheme Photocatalyst. *Nanomaterials* 9, 1706. doi:10.3390/nano9121706

Wang, G., Zhi, Y., Bo, M., Xiao, S., Li, Y., Zhao, W., et al. (2020). 2D Hexagonal Boron Nitride/Cadmium Sulfide Heterostructure as a Promising Water-Splitting Photocatalyst. *Phys. Status Solidi B* 257, 1900431. doi:10.1002/pssb.201900431

Wang, G., Zhang, L., Li, Y., Zhao, W., Kuang, A., Li, Y., et al. (2020). Biaxial Strain Tunable Photocatalytic Properties of 2D ZnO/GeC Heterostructure. *J. Phys. D: Appl. Phys.* 53, 015104. doi:10.1088/1361-6463/ab440e

Wang, G., Li, Z., Wu, W., Guo, H., Chen, C., Yuan, H., et al. (2020). A Two-Dimensional H-Bn/c2n Heterostructure as a Promising Metal-free Photocatalyst for Overall Water-Splitting. *Phys. Chem. Chem. Phys.* 22, 24446–24454. doi:10.1039/d0cp03925j

Wang, G., Gong, L., Li, Z., Wang, B., Zhang, W., Yuan, B., et al. (2020). A Two-Dimensional CdO/CdS Heterostructure Used for Visible Light Photocatalysis. *Phys. Chem. Chem. Phys.* 22, 9587–9592. doi:10.1039/d0cp00876a

Wickramaratne, D., Zahid, F., and Lake, R. K. (2014). Electronic and Thermoelectric Properties of Few-Layer Transition Metal Dichalcogenides. *J. Chem. Phys.* 140, 124710. doi:10.1063/1.4869142

Xie, S., Tu, L., Han, Y., Huang, L., Kang, K., Lao, K. U., et al. (2018). Coherent, Atomically Thin Transition-Metal Dichalcogenide Superlattices with Engineered Strain. *Science* 359, 1131–1136. doi:10.1126/science.aao5360

Xu, Q., Zhang, L., Yu, J., Wageh, S., Al-Ghamdi, A. A., and Jaroniec, M. (2018). Direct Z-Scheme Photocatalysts: Principles, Synthesis, and Applications. *Mater. Today* 21, 1042–1063. doi:10.1016/j.mattod.2018.04.008

Yang, Q., Tan, C.-J., Meng, R.-S., Jiang, J.-K., Liang, Q.-H., Sun, X., et al. (2017). AlN/BP Heterostructure Photocatalyst for Water Splitting. *IEEE Electron. Device Lett.* 38, 145–148. doi:10.1109/led.2016.2633487

Yu, Z., Ong, Z.-Y., Li, S., Xu, J.-B., Zhang, G., Zhang, Y.-W., et al. (2017). Analyzing the Carrier Mobility in Transition-Metal Dichalcogenide MoS2Field-Effect Transistors. *Adv. Funct. Mater.* 27, 1604093. doi:10.1002/adfm.201604093

Zhang, W., and Ji, W. (2020). Two-dimensional van der Waals heterostructure CdO/PtSe2: promising visible light photocatalyst for overall water splitting. *Phys. Chem. Chem. Phys.* 22, 24662–24668. doi:10.1039/d0cp03564e

Zhao, Y., Cui, L., Sun, Y., Zheng, F., and Ke, W. (2019). Ag/CdO NP-Engineered Magnetic Electrochemical Aptasensor for Prostatic Specific Antigen Detection. *ACS Appl. Mater. Inter.* 11, 3474–3481. doi:10.1021/acsami.8b18887

Zheng, Z., Ren, K., Huang, Z., Zhu, Z., Wang, K., Shen, Z., et al. (2021). Remarkably Improved Curie Temperature for Two-Dimensional CrI3 by Gas Molecular Adsorption: a DFT Study. *Semicond. Sci. Technol.* 36, 075015. doi:10.1088/1361-6641/ac01a2

Zheng, R., Ren, K., Yu, J., Zhu, Z., and Sun, Q. (2021). "Type-II Heterostructure Based on Two-Dimensional Arsenene and PtS_2 with Novel Light Absorption Performance," in *Third International Conference on Optoelectronic Science and Materials (ICOSM 2021)* (Hefei: SPIE), 182–186.

Zhu, Z., Ren, K., Shu, H., Cui, Z., Huang, Z., Yu, J., et al. (2021). First-Principles Study of Electronic and Optical Properties of Two-Dimensional WSSe/BSe van der Waals Heterostructure with High Solar-to-Hydrogen Efficiency. *Catalysts* 11, 991. doi:10.3390/catal11080991

Zhuang, H. L., and Hennig, R. G. (2013). Computational Identification of Single-Layer CdO for Electronic and Optical Applications. *Appl. Phys. Lett.* 103, 212102. doi:10.1063/1.4831972

Conflict of Interest: The authors declare that the research was conducted in the absence of any commercial or financial relationships that could be construed as a potential conflict of interest.

Publisher's Note: All claims expressed in this article are solely those of the authors and do not necessarily represent those of their affiliated organizations or those of the publisher, the editors, and the reviewers. Any product that may be evaluated in this article, or claim that may be made by its manufacturer, is not guaranteed or endorsed by the publisher.